Chemical Engineering Science 262 (2022) 118013

Contents lists available at ScienceDirect

Chemical Engineering Science

journal homepage: www.elsevier.com/locate/ces

Effects analysis on soot oxidation performance in the diesel particulate filter based on synergetic passive-active composite regeneration methods

Chao Zhong [a,b,c], Jingwei Liang [c], Yun Zhu [a,c], Hongyan Zuo [a,c,*], Shaoli Wang [b,c], Bo Chen [a,c], Xin Wu [c], Chenxi Wu [c]

[a] Hunan Provincial Key Laboratory of Vehicle Power and Transmission System, Hunan Institute of Engineering, Xiangtan 411104, China
[b] Hunan Engineering Research Center of New Energy Vehicle Lightweight, Hunan Institute of Engineering, Xiangtan 411104, China
[c] School of Mechanical Engineering, Hunan Institute of Engineering, Xiangtan 411104, China

HIGHLIGHTS

- A coupled model of DPF passive and active regeneration is established.
- Control regime transition of DPF regeneration mechanisms is investigated.
- Key parameters affecting soot oxidation mechanisms are summarized.

GRAPHICAL ABSTRACT

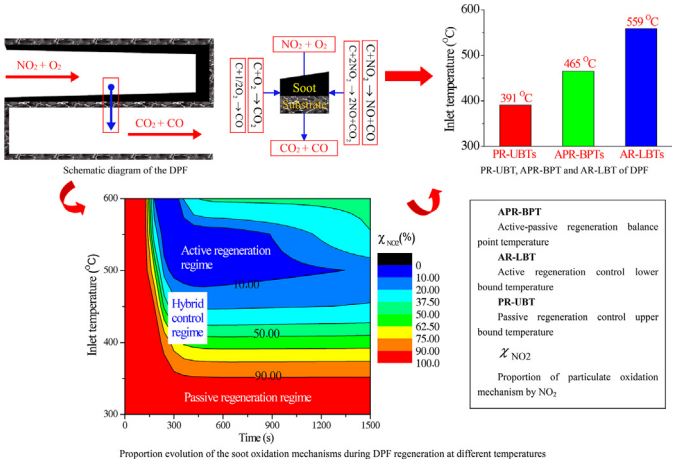

Proportion evolution of the soot oxidation mechanisms during DPF regeneration at different temperatures

ARTICLE INFO

Article history:
Received 11 February 2022
Received in revised form 28 June 2022
Accepted 12 August 2022
Available online 20 August 2022

Keywords:
Diesel particulate filter
Soot oxidation
Active regeneration
Passive regeneration
Composite regeneration
Control regime

ABSTRACT

Diesel particulate filters (DPFs) are standard components to control particulate emissions from diesel engine. Different DPF regeneration mechanisms, including passive regeneration and active regeneration, affect the performance of itself and downstream post-processing equipment. In order to study soot oxidation mechanism in DPF, DPF passive-active coupled regeneration model is established, and its kinetic parameters are verified. Active-passive regeneration balance point temperature (APR-BPT), passive regeneration control upper bound temperature (PR-UBT) and active regeneration control lower bound temperature (AR-LBT) are defined to study-three control regimes affected by two soot oxidation mechanisms. Additionally, the effect analysis of key parameters on APR-BPT, PR-UBT and AR-LBT is conducted to reveal the regeneration regime and the regeneration temperature boundary. The research on the soot combustion mechanisms under the synergetic passive-active composite regeneration of the DPF will provide a theoretical basis for DPF regeneration and its control.

© 2022 Elsevier Ltd. All rights reserved.

* Corresponding author at: Hunan Provincial Key Laboratory of Vehicle Power and Transmission System, Hunan Institute of Engineering, Xiangtan 411104, China.
E-mail address: zuohongyan@hnie.edu.cn (H. Zuo).

https://doi.org/10.1016/j.ces.2022.118013
0009-2509/© 2022 Elsevier Ltd. All rights reserved.

Nomenclature

A	Area [m^2]
a_c	Geometric surface area [$m^2 \cdot m^{-3}$]
c_p	Specific heat capacity [$J \cdot (kg \cdot K)^{-1}$]
d	Channel diameter [m]
D_w	Effective diffusion coefficient [$m^2 \cdot s^{-1}$]
E	Activation energy [$J \cdot mol^{-1}$]
K	Number of components
k	Reaction rate constant [s^{-1}]
k_m	Mass transfer coefficient [$m \cdot s^{-1}$]
k_{soot}	Permeability coefficient of soot layer [m^2]
k_{wall}	Permeability coefficient of wall [m^2]
h	Heat transfer coefficient [$W \cdot m^{-2} \cdot K^{-1}$]
L	Channel length [m]
M_C	Molar mass of carbon [$kg \cdot mol^{-1}$]
M_k	Molar mass of species k [$kg \cdot mol^{-1}$]
p	Pressure [Pa]
r	Reaction rate [$mol \cdot s^{-1} m^{-3}$]
S	Specific surface of the particulate [$m^2 \cdot m^{-3}$]
t	Time[s]
T	Temperature [K]
v	Gas velocity[$m \cdot s^{-1}$]
v_w	Wall velocity [$m \cdot s^{-1}$]
V	Volume [m^3]
y	Mass fraction

Greek letters

τ	Tortuosity
λ	Thermal conductivity [$W \cdot m^{-1} \cdot K^{-1}$]
μ	Viscosity [Pa·s]
ρ	Density [$kg \cdot m^{-3}$]
ρ_{soot}	Particulate density in the channel gas flow [$kg \cdot m^{-3}$]
ζ	Sum
ξ	Pressure drop loss coefficient
χ	Proportion of particulate oxidation mechanism
χ_{O_2}	Proportion of particulate oxidation by O_2
χ_{NO_2}	Proportion of particulate oxidation by NO_2
γ	Stoichiometric coefficient
ε_S	Porosity
δS	Washcoat thickness of washcoat, particulate or filter wall [m]

Subscripts and superscripts

0	Channel entrance
1	Inlet channel
2	Outlet channel
i	Species index
j	Reaction index
g	Gas
w	Washcoat
S	Solid

Abbreviations

APR-BPT	Active-passive regeneration balance point temperature
AR-LBT	Active regeneration control lower bound temperature
DOC	Diesel oxidation catalyst
DPF	Diesel particulate filter
PM	Particulate matter
PR-UBT	Passive regeneration control upper bound temperature

1. Introduction

Although the application of new energy power is now more widely (Huang et al., 2007; Zhao et al., 2020; Zhao et al., 2018), the traditional internal combustion engine is still the main force that cannot be ignored in the transportation market. With the increasingly stringent emission regulations, gasoline engines are developing in the direction of high efficiency and low emissions (Huang et al., 2006). While, diesel engines are still widely used due to greater torque, higher fuel economy and lower carbon dioxide emissions (Wu et al., 2018; Zhong et al., 2019). However, there are particulate matter (PM) emissions problems caused by the diesel engine due to incomplete combustion (Ni et al., 2020; Cheng et al., 2018). Diesel particulate filters (DPFs) are standard components to control particulate emissions from diesel engine (Caliskan and Mori, 2017; Chen and Wang, 2014). The continuous deposition of particles in the DPF causes an increase in the back pressure of the original engine and a decrease in its performance (Mikulic et al., 2010; Zhang et al., 2018), and thus needing to regenerate DPF (Ebrahimnataj et al., 2018). The DPF regeneration is divided into periodic active regeneration and full-time passive regeneration (Bai et al., 2016; Yamada et al., 2017). The active regeneration relies on the mechanism of soot combustion by O_2 at a temperature above 550 ℃, while passive regeneration is based on the mechanism of soot oxidation by NO_2 at relatively low DPF temperature (Chen and Wang, 2012; Gorsmann, 2005). Temperature that triggers active regeneration is increased by means of traditional methods, such as post heaters or fuel late injections or specific post burners located upstream the DPF (Cordtz et al., 2011; Meloni and Palma, 2020), and innovative strategies, including the use of nonthermal plasma (Nguyen et al., 2019; Guo et al., 2020) and the microwaves (Palma et al., 2013; Kurien et al., 2020; Zhang et al., 2016). In view of the diversity of operating characteristics of existing and new engines, active regeneration of diesel particulate filters is essential to improve its performance (Tadrous et al., 2010; Ko et al., 2016). Passive regeneration can increase the durability of the DPF and reduce the fuel loss associated with active regeneration (Tang et al., 2014; Singh et al., 2006). Furthermore, in the DPF regeneration process, soot oxidation by O_2 and NO_2 are a mutual process. Therefore, it is important to simulate the mechanism by which NO_2 and O_2 oxidize particulates since a real-life DPF undergoes both modes of regeneration (Premchand et al., 2013).

Kinetic analysis of soot oxidation by NO_2 and O_2 has been studied extensively (Leistner et al., 2012; Wang-Hansen et al., 2013; Matarrese et al., 2017). D. Smith et al. have conducted experimental research on real-time particulate emissions rates from active and passive heavy-duty DPF regeneration (Smith et al., 2019). Chen et al. have conducted experiment on the active and passive regeneration procedures of a DPF in a diesel methanol dual fuel engine (Chen et al., 2020). The effects of various washcoat technologies under active and passive regeneration conditions was performed using laboratory generated soot on a variety of SiC DPF formulations (Warner et al., 2010). Ishizawa et al. have investigated ash loading and its relationship to DPF active and passive regeneration (Ishizawa et al., 2009). The model has been developed to simulate various rates of NO_2-soot and O_2-soot oxidation at different engine operating conditions (Zhong et al., 2019). The characteristics of composite regeneration including active regeneration and passive regeneration have been studied, which also shows that the soot

oxidation rate is different under different regeneration modes (Jiao et al., 2017; Stanmore et al., 2001). A review article about the soot oxidation with carbon dioxide or nitrogen dioxide of experiments, mechanisms and models has been published by Stanmore et al. (Jacquot et al., 2000). The reactivity of nitrogen dioxide NO_2 towards soot is far greater than that of oxygen at 500 ℃ and the same concentration (0.1 %) (Setiabudi et al., 2004). In the soot-NO_2–O_2 reaction system, soot oxidation with NO_2 is enhanced by the presence of O_2 (Kandylas et al., 2002). Previous studies have analyzed soot combustion mechanisms in DPF, and a few have obtained the change of two soot oxidation mechanisms in DPF regeneration process caused by influencing factors.

However, the existing literature rarely deals with the quantitative representation and effect analysis on the proportion of the soot oxidation mechanisms in the DPF. In order to study the evolution of two soot oxidation mechanisms during synergetic passive-active composite regeneration, this work defines PR-UBT, APR-BPT and AR-LBT for the first time to study the influence of key parameters on the regeneration regime and the regeneration temperature boundary. The research on the regeneration regime and the regeneration temperature boundary during the synergetic passive-active composite regeneration provides a theoretical basis for coupled DPF regeneration and its control.

2. Mathematical model and model validation

2.1. Mathematical model

The one-dimensional modeling is sufficient to meet the requirements of modeling all the channels in the same way (Peters et al., 2004–01-1132; 2004.; Jiang et al., 2016). Fig. 1 shows the schematic diagram of a single channel pair of DPF structure. The model fitted kinetic parameters of DPF passive and active regeneration is capable of describing momentum and heat transfer as well as reaction phenomena in the filter and being applied to actual cycles with time-related soot loading and temperature during the synergetic passive-active composite regeneration.

Considering the impact of entry region, the Sieder-Tate correlation and the Hawthorn relation are respectively used to calculate heat transfer and mass transfer between the fluid in the channel and the filter wall. The remaining assumptions of the DPF model during the synergetic passive-active composite regeneration are expressed as follows:

(1) uniform distribution of flow at inlet, material and catalyst across all the channels; (2) negligible axial diffusion in the gas phase; (3) completely insulated outer wall in the radial direction; (4) negligible heat capacity and thermal conductivity of the gas in wall; (5) the particulate deposition in inlet channel is consistent with the axial flow distribution; (6) the particulate matter is assumed to be soot.

Based on the above assumptions, the main governing equations of the single channel model in the DPF during the synergetic passive-active composite regeneration are expressed as follows:

(1) Mass conservation equation for the gas species in the channels.

$$\frac{\partial\left(\rho_1 y_{i,1} d_1^2(z,t)\right)}{\partial t}+\frac{\partial\left(d_1^2(z,t)\rho_1 v_1 y_{i,1}\right)}{\partial z}=-4d_1(z,t)\rho_1 v_{S,1} y_{i,1} \tag{1}$$

$$\frac{\partial(\rho_2 y_{i,2})}{\partial t}+\frac{\partial(\rho_2 v_2 y_{i,2})}{\partial z}=\frac{4}{d}\rho_2 v_{S,2} y_{i,2} \tag{2}$$

$$d_1(z,t)\rho_1 v_{S,1} y_{i,1}+d\delta_S\rho_{g,S} v_S y_{i,1}\left(1-\exp\left(-a_c\sum_{j=1}^{K}\varsigma_{i,j} r_j \delta_S / v_{S,1} y_{i',1}\right)\right) = d\rho_2 v_{S,2} y_{i,2} \tag{3}$$

$$d_1(z,t)=d-2\delta_{soot}(z,t)=\sqrt{d^2-\frac{m}{n_{channel} L r_{soot}}} \tag{4}$$

$$\rho_2 v_{S,2} d=\rho_1 v_{S,1} d_1(z,t) \tag{5}$$

where S stands for particulate or filter wall, and i' stands for NO_2 or O_2.

(2) Axial momentum conservation equation for the gas species in the channels.

$$\frac{\partial(\rho_1 v_1)}{\partial t}+\frac{\partial(\rho_1 v_1^2)}{\partial z}=-\frac{\partial p_1}{\partial z}-F\mu v_1-\frac{1}{d_1(z,t)}\rho_1 v_{S,1}^2 \tag{6}$$

$$\frac{\partial(\rho_2 v_2)}{\partial t}+\frac{\partial(\rho_2 v_2^2)}{\partial z}=-\frac{\partial p_2}{\partial z}-\frac{F\mu v_2}{d^2}+\frac{1}{d}\rho_2 v_{S,2}^2 \tag{7}$$

(3) Enthalpy balance equation for the gas species in the channels.

$$\frac{\partial\left(d_1^2(z,t)\rho_1 c_{p,g} T_1\right)}{\partial t}+\frac{\partial\left(d_1^2(z,t)\rho_1 v_1 c_{p,g} T_1\right)}{\partial z} = 4d_1(z,t)\left(h_1(T_S-T_1)-\rho_1 v_{S,1} c_{p,g} T_S\right) \tag{8}$$

$$\frac{\partial(\rho_2 T_2)}{\partial t}+\frac{\partial(\rho_2 v_2 T_2)}{\partial z}=\frac{4}{d}\left(\frac{1}{c_{p,g}}h_2(T_S-T_2)+\rho_2 v_{S,2} T_S\right) \tag{9}$$

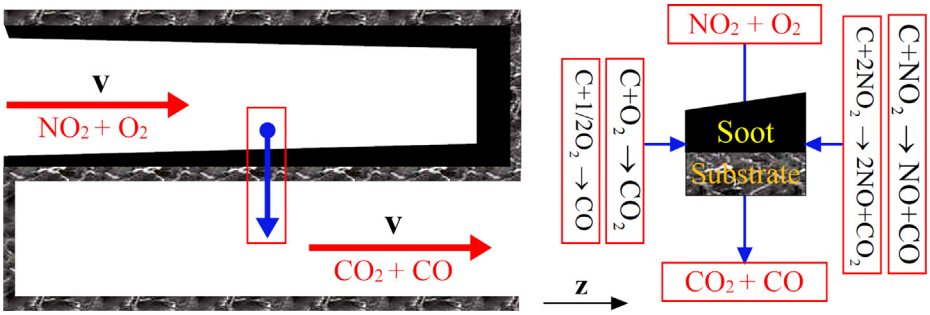

Fig. 1. Schematic physical diagram of DPF structure.

(4) Enthalpy balance equation of the solid phase.

$$\rho_s c_{p,s}\frac{\partial(1-\varepsilon_S)T_S}{\partial t} = (1-\varepsilon_S)\lambda_S\frac{\partial^2 T_S}{\partial z^2} + \sum_{i=1}^{J}\Delta_r H_{mj}(T)r_j + h_1 a_c(T_1 - T_S) + h_2 a_c(T_2 - T_S) + c_{p,g}T_S(\rho_1 v_{S,1} - \rho_2 v_{S,2}) \tag{10}$$

(5) Soot mass balance equation.

$$\frac{\partial m}{\partial t} = -\frac{M_C \cdot d}{M_{i'}}\int_0^L \rho_{g,S} v_S y_{i',1}\left(1 - \exp\left(-S\sum_{j=1}^{K}\varsigma_{i',j}r_j\delta_S / v_S y_{i',1}\right)\right)dz + 4d_1(z,t)L(\rho_1 v_1 y_{soot}|_{z=0})\eta \tag{11}$$

where η is calculated in our previous work (Zouaoui et al., 2014).

The control equations solved with boundary and initial conditions:

$$\begin{cases} z = 0, v_1 = v_0, T_1 = T_0, v_2 = 0, \partial T_S/\partial z = 0 \\ z = L, v_1 = 0, p_2 = p_{atm}, \partial T_S/\partial z = 0 \\ t = 0, v_1 = v_2 = 0, p_1 = p_2 = p_{atm}, d_1 = d_2 = d \end{cases} \tag{12}$$

2.2. Model validation

For modeling convenience, except for O_2 and NO_2, the effect of other exhaust components on the soot oxidation during the synergetic passive-active composite regeneration is negligible and the oxidation reaction order with respect to O_2 and NO_2 is first-order (Lee et al., 2008). The kinetic parameters of active regeneration and passive regeneration are separately from literature (Lee et al., 2009; Konstandopoulos and Kostoglou, 2000). Furthermore; the values of other parameters are: K_f = 0.02, q_f = 0.21, E_f / R = 3000 K (Miyairi, et al., 2001).

$$C + 1/2O_2 \rightarrow CO \tag{13}$$

$$C + O_2 \rightarrow CO_2 \tag{14}$$

$$C + NO_2 \rightarrow NO + CO \tag{15}$$

$$C + 2NO_2 \rightarrow 2NO + CO_2 \tag{16}$$

The reaction rate expressions during the synergetic passive-active composite regeneration are expressed as follows:

$$r_1 = f_{co}K_1 e^{\left(\frac{-E_1}{RT}\right)}y_{O_2} \tag{17}$$

$$r_2 = (1 - f_{CO})r_1/f_{CO} \tag{18}$$

$$r_3 = K_3 e^{\left(\frac{-E_3}{RT}\right)}y_{NO_2} \tag{19}$$

$$r_4 = K_4 e^{\left(\frac{-E_4}{RT}\right)}y_{NO_2} \tag{20}$$

and

$$f_{CO} = \frac{1}{1 + K_f y_{CO}^{q_f} e^{E_f/RT}} \tag{21}$$

As shown in Fig. 2, after the temperature reached 600 °C (t greater than 200 s), the calculated values agree well with the experimental values (Triana, 2005), indicating that the kinetics parameters of the thermal regeneration reaction are applicable to the model. During the preheating phase of the DPF (t less than 200 s), a large error in the wall temperature of the DPF rear section corresponds to the deviated heat transfer of the system in the model. In order to verify the kinetic model of DPF passive regeneration, under specific working conditions and DPF structure, the calculated value of soot loading during the DPF regeneration process is compared with the experimental value (Zhang et al., 2021), as shown in Fig. 3. These results indicate the ability of the DPF model to reliably predict the soot loading during DPF passive regeneration.

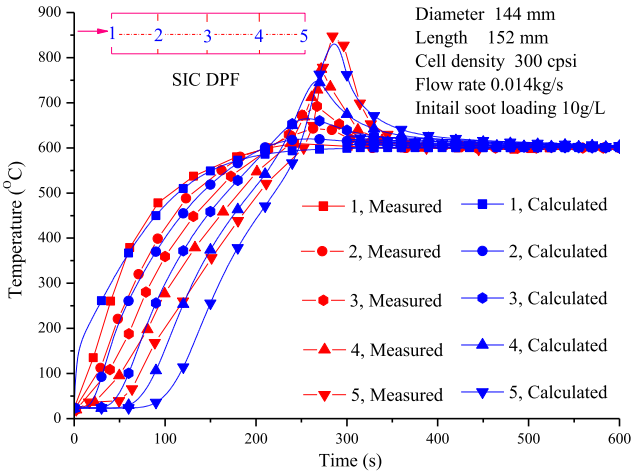

Fig. 2. Comparison of the calculated and measured (Triana, 2005) wall temperatures for active regeneration.

3. Results and discussions

The proportion of soot oxidized by O_2 and NO_2 is calculated as shown in Eq. (22) and Eq. (23), respectively. The average proportion of soot oxidized by O_2 is calculated as shown in Eq. (24). The PR-UBT, APR-BPT and AR-LBT are presented in Eq. (25), Eq. (26) and Eq. (27), respectively. The calculation method of PR-UBT, APR-BPT and AR-LBT is to first calculate the proportion of soot oxidation mechanisms in a wide range of temperatures, and then narrow the range in subsequent calculations until the calculated temperature is at PR-UBT, APR-BPT or AR-LBT. If the temperature range ($T_1 \sim T_2$) is reduced to 1 °C, and the proportion of soot oxidized by O_2 is less than the specified standard value (10 %, 50 % or 90 %) at the temperature T_1, while the calculated value is greater at the temperature T_2, it is stipulated that at which temperature (T_1 or T_2) the absolute value of the difference between the proportion of soot oxidation mechanism and the specified standard value is less, the temperature is recognized as PR-UBT, APR-BPT or AR-LBT. In addition, if a certain soot oxidation mechanism accounts for more than 90 %, the DPF regeneration is in the control of the active or passive regeneration regime. While the proportion is less than 10 %, the regeneration method is negligible. When the proportion of the two soot oxidation mechanisms is 10 %-90 %, the DPF regeneration is in the hybrid regeneration regime.

$$\chi_{O_2} = \frac{\int_0^L (2r_1 + r_2)dz}{\int_0^L (2r_1 + r_2 + r_3 + 0.5r_4)dz} \tag{22}$$

$$\chi_{NO_2} = \frac{\int_0^L (r_3 + 0.5r_4)dz}{\int_0^L (2r_1 + r_2 + r_3 + 0.5r_4)dz} \tag{23}$$

where r_1, r_2, r_3 and r_4 are expressed as Equations (17) to (21), respectively.

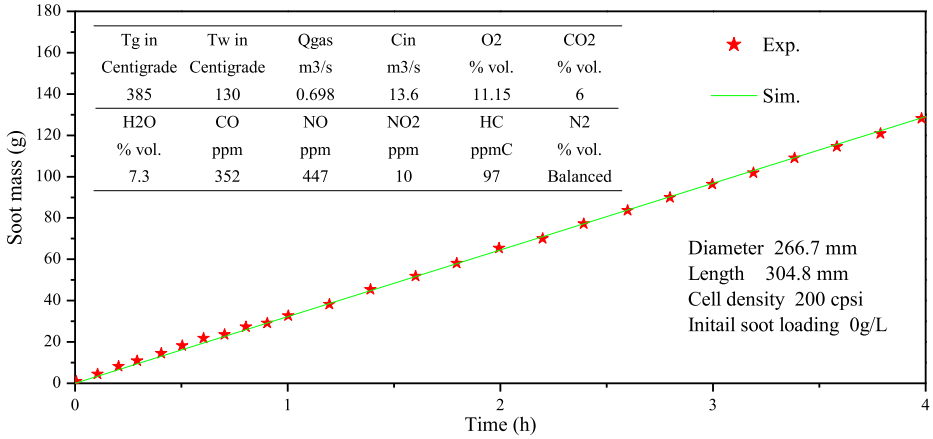

Fig. 3. Comparison of the calculated and measured (Zhang et al., 2021) soot mass for passive regeneration.

$$\overline{\chi_{O_2}}(T) = \int_0^{t_{AP}} \int_0^{L} \left(\frac{K_3 e^{\left(\frac{-E_3}{RT}\right)} y_{NO_2} + 0.5K_4 e^{\left(\frac{-E_4}{RT}\right)} y_{NO_2}}{f_{co} K_1 e^{\left(\frac{-E_1}{RT}\right)} y_{O_2} + K_3 e^{\left(\frac{-E_3}{RT}\right)} y_{NO_2} + 0.5K_4 e^{\left(\frac{-E_4}{RT}\right)} y_{NO_2}} \right) dz dt \times 100\% \quad (24)$$

where t_{AP} is the limitation time, which is defined as the time it takes for 99 % of the soot to be consumed or to reach a balance between soot deposition and soot consumption.

Let T = PR-UBT, APR-BPT or AR-LBT, then:

$$\overline{\chi_{O_2}}(PR-UBT) = 10\% \quad (25)$$

$$\overline{\chi_{O_2}}(APR-BPT) = 50\% \quad (26)$$

$$\overline{\chi_{O_2}}(AR-LBT) = 90\% \quad (27)$$

As shown in Fig. 4(a), before 100 s, because of the thermal resistance upstream of the DPF, the reaction of soot with NO_2 and O_2 is extremely slow, but the former has a higher reaction rate. Therefore, the soot oxidation is in the control of passive regeneration regime. After 100 s, when the inlet temperature is low (≤350℃), the reactivity of NO_2 towards soot is far greater than that of O_2, and thus the proportion of soot oxidized by NO_2 exceeds 90 %. Therefore, the DPF is under passive regeneration control. When the inlet temperature is high (≥400℃), soot-O_2 reaction is accelerated, and the soot oxidation will enter the hybrid regeneration regime successively. And as the temperature rises, the faster it will enter the hybrid regeneration regime. When the inlet temperature is 400 °C or 450 °C, the soot oxidation only enters the hybrid regeneration regime; while at the inlet temperature of 500 °C, 550 °C or 600 °C, the soot oxidation enters the hybrid regeneration regime first, and then the proportion of soot oxidized by O_2 exceeds 90 %, entering the active regeneration regime, and finally enters the hybrid regeneration regime again. It may be because with the decreased particulate concentration in the DPF, although the oxygen concentration in the exhaust is greater than the NO_2 concentration, the pre-exponential factor of the soot-NO_2 reaction in the model is greater than that of soot-O_2 reaction. Therefore, the rate of soot oxidation by NO_2 increases, and the proportion of soot oxidation by O_2 mechanism decreases. As shown in Fig. 4(b) and 4(c), as DPF regeneration continues, when the inlet temperature is low (≤350℃), DPF is still under the control of passive regeneration. When the inlet temperature is 400℃, the proportion of soot oxidation by NO_2 mechanism increases until it exceeds 90 %, and thus the DPF regeneration is in the passive regeneration regime. When the inlet temperature is higher than 450℃, the proportion of soot oxidation by NO_2 mechanism increases but does not exceed 90 %, and the proportion of soot oxidation by O_2 mechanism decreases but does not less than 10 %, and thus the soot oxidation is in the hybrid regeneration regime. In addition, when the regeneration time is long enough, the particulates are continuously consumed and deposited, and the proportion of the soot oxidation by NO_2 and O_2 will tend to an asymptotic value.

The PR-UBTs, APR-BPTs and AR-LBTs of the DPF at different inlet O_2 concentration are shown in Fig. 5. When the inlet oxygen concentration is 5 %, 10 %, and 15 %, the passive regeneration regime is ~ 391℃, ~372℃ and ~ 344℃, respectively; the hybrid regeneration regime is 391 ~ 559℃, 372 ~ 525℃ and 344 ~ 514℃, respectively; the active regeneration regime is 559℃~, 525℃~ and 514℃~, respectively. With the increase of inlet O_2 concentration, PR-UBTs, APR-BPTs and AR-LBTs decrease, the passive regeneration regime is narrowed, while the active regeneration regime is expanded. It shows that as the inlet O_2 concentration increases, the proportion of soot oxidation by NO_2 mechanism decreases and the proportion of soot oxidation by O_2 mechanism increases. This is because the increase in inlet O_2 concentration is beneficial to the soot-O_2 reaction, but has very limited effect on the soot-NO_2 reaction.

The PR-UBTs, APR-BPTs and AR-LBTs of the DPF at different inlet flow rates are shown in Fig. 6. When the inlet flow rate is 0.007 kg/s, 0.014 kg/s and 0.021 kg/s, the passive regeneration regime is ~ 358℃, ~372℃ and ~ 381℃, respectively; the hybrid regeneration regime is 358 ~ 512℃, 372 ~ 525℃ and 381 ~ 537℃, respectively; the active regeneration regime is 512℃~, 525℃~ and 537℃~, respectively. With increasing inlet flow rate, PR-UBTs, APR-BPTs and AR-LBTs increase, the passive regeneration regime expands, while the active regeneration regime narrows. It shows that with the increase of the inlet flow rate, the proportion of soot oxidation by NO_2 mechanism increases and the proportion of soot oxidation by O_2 mechanism decreases. This is because in a relatively fast reaction, although the increase in flow rate is not conducive to the full contact of the reactant gas and the particulates, the amount of O_2 and NO_2 flowing through the particulate layer and the filter wall per unit time increases. However, it is possible that for a given concentration of O_2 and NO_2, soot oxidation by O_2 (Eq. (12) and Eq. (13)) needs more carbon (soot) than soot oxidation by NO_2 (Eq. (14) and Eq. (15)). Thus, the lesser the remaining soot mass in the filter surface, the lesser the weight of O_2-assisted oxidations, compared to NO_2-assisted.

The diesel oxidation catalyst (DOC) located in upstream of the DPF will increase the inlet NO_2 concentration of the DPF [52]. Therefore, it is important to study the influence of the large inlet NO_2 concentration on the proportion of the regeneration mechanism. Increasing NO_X concentration and NO_2/NO_X ratio at

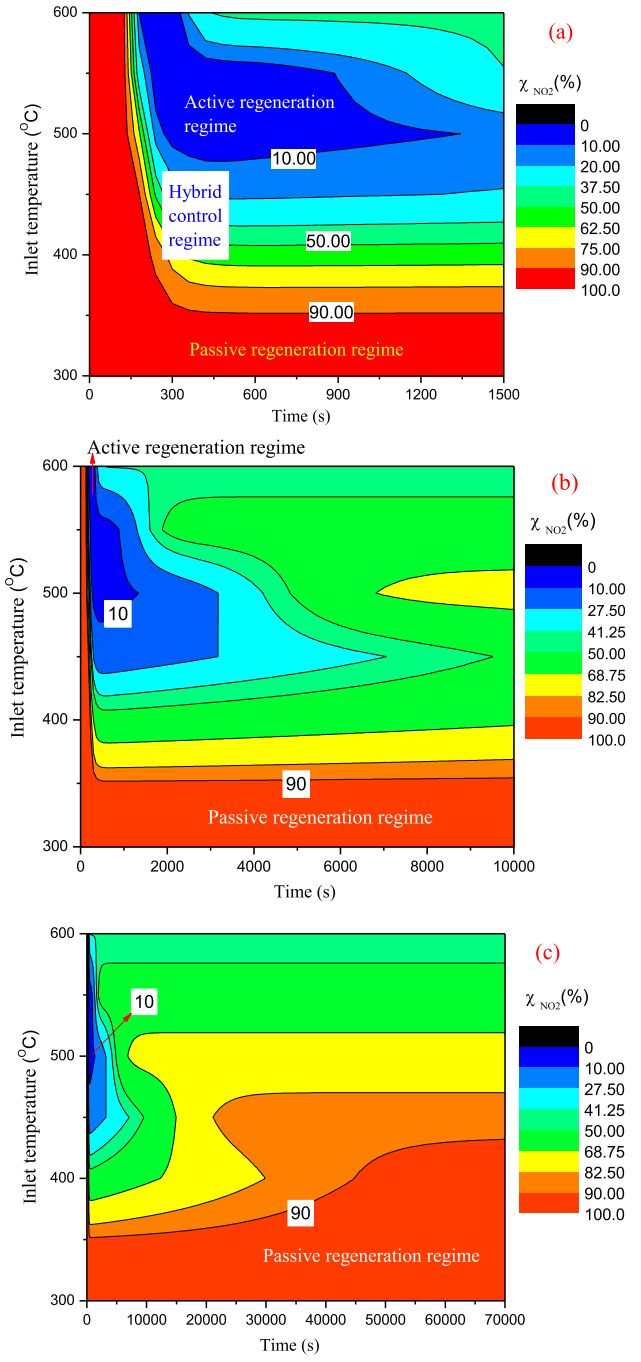

Fig. 4. Proportion evolution of the soot oxidation mechanism in DPF at different temperatures (a) First 1500 s; (b) First 10,000 s; (c) 70,000 s (10 % O_2, 0.014 kg/s, 10 %NO_2/NO_X, 10 g/L initial soot loading).

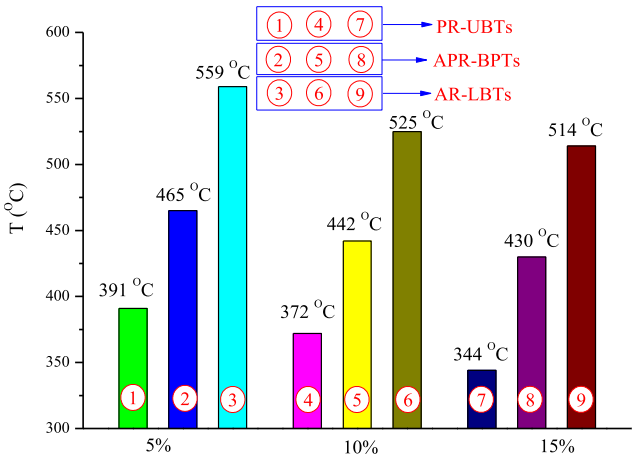

Fig. 5. PR-UBTs, APR-BPTs and AR-LBTs under different inlet O_2 concentration.

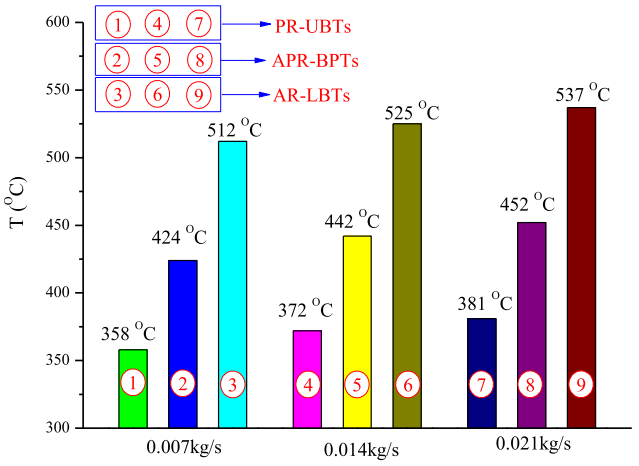

Fig. 6. PR-UBTs, APR-BPTs and AR-LBTs under different inlet flow rate.

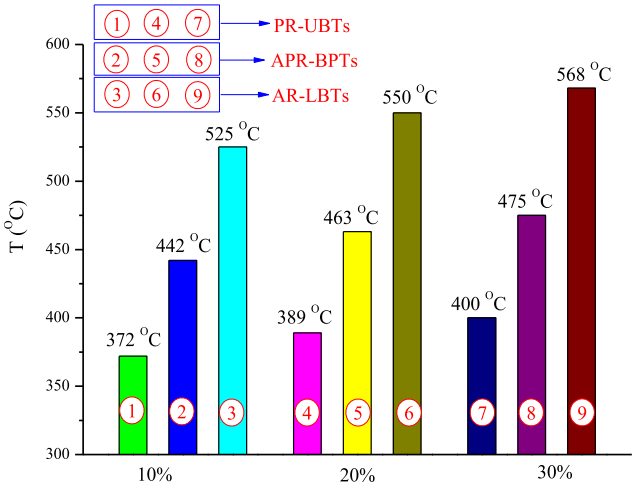

Fig. 7. PR-UBTs, APR-BPTs and AR-LBTs under different inlet NO_2/NO_X ratio.

aftertreatment system both increase the inlet NO_2 concentration of the DPF. Therefore, only the increase in the NO_2/NO_X ratio has been discussed here. The PR-UBTs, APR-BPTs and AR-LBTs of the DPF at different inlet NO_2/NO_X ratios are shown in Fig. 7. When the inlet NO_2/NO_X ratio is 10 %, 20 %, and 30 %, the passive regeneration regime is ~ 372℃, ~389℃ and ~ 400℃, respectively; the hybrid regeneration regime is 372 ~ 525℃, 389 ~ 550℃ and 400 ~ 568℃, respectively; the active regeneration regime is 525℃~, 550℃~ and 568℃, respectively. With the increase of inlet NO_2/NO_X ratio, PR-UBTs, APR-BPTs and AR-LBTs increase, the passive regeneration regime enlarges, and the active regeneration regime diminishes. It shows that as the inlet NO_2/NO_X ratio increases, the proportion of soot oxidation by NO_2 mechanism increases and the proportion of soot oxidation by O_2 mechanism decreases. This is because the increase in the inlet NO_2/NO_X ratio increases the concentration of inlet NO_2, which is beneficial to the soot-NO_2 reaction, but has no effect on the soot-O_2 reaction.

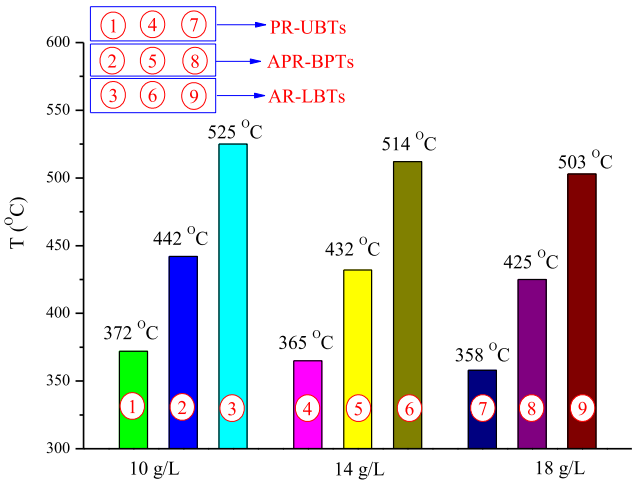

Fig. 8. PR-UBTs, APR-BPTs and AR-LBTs under different initial soot loading.

The PR-UBTs, APR-BPTs and AR-LBTs of the DPF at different initial soot loading are shown in Fig. 8. When the initial soot loading is 10 g/L, 14 g/L, and 18 g/L, the passive regeneration regime is ~ 372℃, ~365℃ and ~ 358℃, respectively; the hybrid regeneration regime is 372 ~ 525 °C, 365 ~ 514 °C and 358 ~ 503 °C, respectively; the active regeneration regime is 525 °C~, 514 °C ~ and 503 °C~, respectively. With the increase of the initial soot loading, PR-UBTs, APR-BPTs and AR-LBTs decrease, the passive regeneration regime narrows, and the active regeneration regime expands. It shows that as the initial soot loading increases, the proportion of soot oxidation by NO_2 mechanism decreases and the proportion of soot oxidation by O_2 mechanism increases. This is because the O_2 concentration in exhaust is much greater than the NO_2 concentration, and the increase in the initial soot loading results in the faster soot-O_2 reaction while a small impact on the soot-NO_2 reaction.

4. Conclusions

Different DPF regeneration mechanisms, including passive regeneration and active regeneration, affect the performance of itself and downstream post-processing equipment. In order to study soot combustion mechanism in DPF, a coupled model of DPF passive and active regeneration is established, and its kinetic parameters are verified. APR-BPT, PR-UBT and AR-LBT are defined for the first time to study-three control regimes. The three control regimes, including the passive regeneration regime, the hybrid regeneration regime and the active regeneration regime, are affected by two soot oxidation mechanisms (soot oxidation by NO_2 and soot combustion by O_2). Additionally, the effect analysis of key parameters on APR-BPT, PR-UBT and AR-LBT is conducted to reveal the evolution of the two soot oxidation mechanisms. The main results show that with increase of the initial soot loading and inlet O_2 concentration, PR-UBTs, APR-BPTs and AR-LBTs decrease, the passive regeneration regime narrows, and the active regeneration regime expands. It means the proportion of soot oxidation by NO_2 mechanism decreases and the proportion of soot oxidation by O_2 mechanism increases. While, the increase of inlet flow rate and inlet NO_2/NO_X ratio respond to the opposite trend. The research on the soot combustion mechanism during DPF regeneration provides a theoretical basis for coupled DPF regeneration and its control. The future work will focus on heating time control during soot combustion process inside DPF.

CRediT authorship contribution statement

Chao Zhong: Resources, Project administration, Software, Data curation, Writing – original draft, Writing – review & editing. **Jingwei Liang:** Software, Data curation, Writing – review & editing. **Yun Zhu:** Software, Data curation, Writing – review & editing. **Hongyan Zuo:** Supervision, Conceptualization, Writing – review & editing. **Shaoli Wang:** Data curation, Writing – review & editing. **Bo Chen:** Writing – review & editing. **Xin Wu:** Writing – review & editing. **Chenxi Wu:** Writing – review & editing.

Data availability

Data will be made available on request.

Declaration of Competing Interest

The authors declare that they have no known competing financial interests or personal relationships that could have appeared to influence the work reported in this paper.

Acknowledgements

The authors thank the financial support of the Scientific Research Fund of Hunan Provincial Education Department (Nos. 21C0584 and 20A107) and Natural Science Foundation in Hunan province (No. 2020JJ4241).

References

Bai, S., Tang, J., Wang, G., Li, G., 2016. Soot loading estimation model and passive regeneration characteristics of DPF system for heavy-duty engine. Appl. Therm. Eng. 100, 1292–1298.
Caliskan, H., Mori, K., 2017. Environmental, enviroeconomic and enhanced thermodynamic analyses of a diesel engine with diesel oxidation catalyst (DOC) and diesel particulate filter (DPF) after treatment systems. Energy 128, 128–144.
Chen, P., Wang, J., 2012. Control-oriented modeling and observer-based estimation of solid and gas temperatures for a diesel engine aftertreatment system. J. Dyn. Syst. Meas. Contr. 134, 061011.
Chen, P., Wang, J., 2014. Air-fraction modeling for simultaneous diesel engine NOx and PM emissions control during active DPF regenerations. Appl. Energy 122, 310–320.
Chen, C., Yao, A., Yao, C., Qu, G., 2020. Experimental study of the active and passive regeneration procedures of a diesel particulate filter in a diesel methanol dual fuel engine. Fuel 264, 116801. https://doi.org/10.1016/j.fuel.2019.116801.
Cheng, Y., Liu, J., Zhao, Z., Song, W., Wei, Y., 2018. A new 3DOM Ce-Fe-Ti material for simultaneously catalytic removal of PM and NO_x from diesel engines. J. Hazard. Mater. 342, 317–325.
Cordtz R, Ivarsson A, Schramm J. Steady state investigations of DPF soot burn rates and DPF modeling. No. 2011-24-0181. SAE Technical Paper, 2011.
Ebrahimnataj, M.R., Ehteram, M.A., Sahebi, M., Abdolmaleki, S., 2018. Numerical and experimental study on the gaseous emission and back pressure during regeneration of diesel particulate filters. Transport. Res. Part D Transport Environ. 62, 11–26.
Görsmann C. Catalytic coatings for active and passive diesel particulate filter regeneration. Monatshefte für Chemie/Chemical Monthly 2005; 136: 91–105.
Guo, X., Ha, K.H., Du, D., 2020. New Experiment of Diesel Exhaust Treatment by Atmospheric Pressure Plasma-Wood Fiber Combination. Catalysts 10 (5), 577. https://doi.org/10.3390/catal10050577.
Huang, Z.H., Ren, Y., Jiang, D.M., Liu, L.X., Zeng, K., Liu, B., Wang, X.B., 2006. Combustion and emission characteristics of a compression ignition engine fuelled with diesel-dimethoxy methane blends. Energy Convers. Manage. 47 (11-12), 1402–1415.
Huang, Z., Wang, J., Liu, B., Zeng, K., Yu, J., Jiang, D., 2007. Combustion characteristics of a direct-injection engine fueled with natural gas-hydrogen blends under different ignition timings. Fuel 86 (3), 381–387.
Ishizawa, T., Yamane, H., Satoh, H., Sekiguchi, K., Arai, M., Yoshimoto, N., Inoue, T., 2009. Investigation into Ash Loading and Its Relationship to DPF Regeneration Method. SAE Int. J. Commer. Veh. 2 (2), 164–175.
Jacquot F, Logie V, Brilhac JF, Gilot P. Comparison of soot reactivity in the presence of oxygen or NO_2. In: Nanoparticle Congress of ETH, Zurich, 2000, August.
Jiang, J., Gong, J., Liu, W., Chen, T., Zhong, C., 2016. Analysis on filtration characteristic of wall-flow filter for ash deposition in cake. J. Aerosol Sci. 95, 73–83.

Jiao, P., Li, Z., Shen, B., Zhang, W., Kong, X., Jiang, R., 2017. Research of DPF regeneration with NOx-PM coupled chemical reaction. Appl. Therm. Eng. 110, 737–745.
Kandylas, I.P., Haralampous, O.A., Koltsakis, G.C., 2002. Diesel soot oxidation with NO_2: engine experiments and simulations. Ind. Eng. Chem. Res. 41 (22), 5372–5384.
Ko, J., Si, W., Jin, D., Myung, C.-L., Park, S., 2016. Effect of active regeneration on time-resolved characteristics of gaseous emissions and size-resolved particle emissions from light-duty diesel engine. J. Aerosol. Sci. 91, 62–77.
Konstandopoulos, A.G., Kostoglou, M., 2000. Reciprocating flow regeneration of soot filters. Combust. Flame 121 (3), 488–500.
Kurien, C., Srivastava, A.K., Gandigudi, N., Anand, K., 2020. Soot deposition effects and microwave regeneration modelling of diesel particulate filtration system. J. Energy Inst. 93, 463–473.
Lee, S.J., Jeong, S.J., Kim, W.S., Lee, C.B., 2008. Computational study on the effects of volume ratio of DOC/DPF and catalyst loading on the PM and NO_x emission control for heavy-duty diesel engines. Int. J. Automot. Technol. 9 (6), 659–670.
Lee, S.-J., Jeong, S.-J., Kim, W.-S., 2009. Numerical design of the diesel particulate filter for optimum thermal performances during regeneration. Appl. Energy 86 (7-8), 1124–1135.
Leistner, K., Nicolle, A., Da Costa, P., 2012. Detailed Kinetic Analysis of Soot Oxidation by NO_2, NO, and NO+O_2. J. Phys. Chem. C 116 (7), 4642–4654.
Matarrese, R., Castoldi, L., Lietti, L., 2017. Oxidation of model soot by NO_2 and O_2 in the presence of water vapor. Chem. Eng. Sci. 173, 560–569.
Meloni, E., Palma, V., 2020. Most Recent Advances in Diesel Engine Catalytic Soot Abatement: Structured Catalysts and Alternative Approaches. Catalysts. 10 (7), 745.
Mikulic I, Zhan R, Eakle S. Dependence of fuel consumption on engine backpressure generated by a DPF. No. 2010-01-0535. SAE Technical Paper, 2010.
Miyairi, Yukio, et al. Numerical study on forced regeneration of wall-flow diesel particulate filters. No. 2001-01-0912. SAE Technical Paper, 2001.
Nguyen, V.T., Nguyen, D.B., Heo, I., Mok, Y.S., 2019. Plasma-Assisted Selective Catalytic Reduction for Low-Temperature Removal of NOx and Soot Simulant. Catalysts 9 (10), 853. https://doi.org/10.3390/catal9100853.
Ni, P., Wang, X., Li, H.u., 2020. A review on regulations, current status, effects and reduction strategies of emissions for marine diesel engines. Fuel 279, 118477. https://doi.org/10.1016/j.fuel.2020.118477.
Palma, V., Ciambelli, P., Meloni, E., 2013. Catalyst Load Optimization for Microwave Susceptible Catalysed DPF. Chem. Eng. Trans. 32, 799–804.
Peters BJ, Wanker RJ, Menzer A, Wurzenberger JC. Intergrated 1D to 3D simulation workflow of exhaust aftertreatment devices. SAE paper 2004-01-1132; 2004.
Premchand K C, Johnson J H, Yang S L. Development of a 1-D catalyzed diesel particulate filter model for simulation of the oxidation of particulate matter and gaseous species during passive oxidation and active regeneration. No. 2013-01-1574. SAE Technical Paper, 2013.
Setiabudi, A., Makkee, M., Moulijn, J.A., 2004. The role of NO_2 and O_2 in the accelerated combustion of soot in diesel exhaust gases. Appl. Catal. B 50 (3), 185–194.
Singh, P., Thalagavara, A.M., Naber, J.D., et al., 2006. An Experimental Study of Active Regeneration of an Advanced Catalyzed Paniculate Filter by Diesel Fuel Injection Upstream of an Oxidation Catalyst. SAE Trans., 334–357
Smith, J.D., Ruehl, C., Burnitzki, M., Sobieralski, W., Ianni, R., Quiros, D., Hu, S., Chernich, D., Collins, J., Huai, T., Dwyer, H., 2019. Real-time particulate emissions rates from active and passive heavy-duty diesel particulate filter regeneration. Sci. Total Environ. 680, 132–139.
Stanmore, B.R., Brilhac, J.F., Gilot, P., 2001. The oxidation of soot: a review of experiments, mechanisms and models. Carbon 39 (15), 2247–2268.
Tadrous T N, Brown K, Towgood P, et al. Development of passive/active DPF system utilizing syngas regeneration strategy-retrofit, real life optimization and performance experience. No. 2010-01-0560. SAE Technical Paper, 2010.
Tang, T., Zhang, J., Cao, D., Shuai, S., Zhao, Y., 2014. Experimental study on filtration and continuous regeneration of a particulate filter system for heavy-duty diesel engines. J. Environ. Sci. 26 (12), 2434–2439.
Triana, A. P. (2005). Development of Models to Study the Emissions, Flow, Kinetic Characteristics Form a Diesel Oxidation Catalyst and Particulate Filter. Ph.D. Disser-tation. Michigan Technological University. USA.
Wang-Hansen, C., Soltani, S., Andersson, B., 2013. Kinetic Analysis of O_2- and NO_2-Based Oxidation of Synthetic Soot. J. Phys. Chem. C 117 (1), 522–531.
Warner, J.R., Dobson, D., Cavataio, G., 2010. A study of active and passive regeneration using laboratory generated soot on a variety of SiC diesel particulate filter formulations. SAE Int. J. Fuels Lubr. 3 (1), 149–164.
Wu, T., Shen, Q., Xu, M., Peng, T., Ou, X.M., 2018. Development and application of an energy use and CO_2 emissions reduction evaluation model for China's online car hailing services. Energy 154, 298–307. https://doi.org/10.1016/J.ENERGY.2018.04.130.
Yamada, H., Inomata, S., Tanimoto, H., 2017. Mechanisms of increased particle and VOC emissions during DPF active regeneration and practical emissions considering regeneration. Environ. Sci. Technol. 51 (5), 2914–2923.
Zhang, B., E, J., Gong, J., Yuan, W., Zuo, W., Li, Y.u., Fu, J., 2016. Multidisciplinary design optimization of the diesel particulate filter in the composite regeneration process. Appl. Energy 181, 14–28.
Zhang, J., Wong, V.W., Shuai, S., Chen, Y.u., Sappok, A., 2018. Quantitative estimation of the impact of ash accumulation on diesel particulate filter related fuel penalty for a typical modern on-road heavy-duty diesel engine. Appl. Energy 229, 1010–1023.
Zhang, Z., Ye, J., Tan, D., Feng, Z., Luo, J., Tan, Y., Huang, Y., 2021. The effects of Fe_2O_3 based DOC and SCR catalyst on the combustion and emission characteristics of a diesel engine fueled with biodiesel. Fuel 290, 120039. https://doi.org/10.1016/j.fuel.2020.120039.
Zhao, X., E, J., Zhang, Z., Chen, J., Liao, G., Zhang, F., Leng, E., Han, D., Hu, W., 2020. A review on heat enhancement in thermal energy conversion and management using Field Synergy Principle. Appl. Energy 257, 113995. https://doi.org/10.1016/j.apenergy.2019.113995.
Zhao, D., Gutmark, E., de Goey, P., 2018. A review of cavity-based trapped vortex, ultra-compact, high-g, inter-turbine combustors. Prog. Energ Combust. 66, 42–82.
Zhong, C., Gong, J., Tan, L., Liu, W., Liu, G., Zhang, Z., 2019. Modeling intraphase and interphase mass transfer limitations for NH_3–SCR over Cu–ZSM–5. Chem. Eng. Sci. 207, 479–489.
Zhong, C., Gong, J., Liu, W., Liu, G., 2019. Low temperature, medium temperature and high temperature performance of the continuous regenerative diesel particulate filter assisted by electric regeneration. Chem. Eng. Sci. 207, 980–992.
Zouaoui, N., Labaki, M., Jeguirim, M., 2014. Diesel soot oxidation by nitrogen dioxide, oxygen and water under engine exhaust conditions: Kinetics data related to the reaction mechanism. C. R. Chim. 17 (7-8), 672–680.